A magnetic circular dichroism and optically detected magnetic resonance investigation of Fe^{2+} and Fe^{3+} centres in $KTaO_3$

2000 J. Phys.: Condens. Matter 12 10599

(http://iopscience.iop.org/0953-8984/12/50/320)

J. Phys.: Condens. Matter **12** (2000) 10599–10610. Printed in the UK PII: S0953-8984(00)17118-8

A magnetic circular dichroism and optically detected magnetic resonance investigation of Fe^{2+} and Fe^{3+} centres in $KTaO_3$

H J Reyher, N Hausfeld and M Pape

FB Physik, Universität Osnabrück, D-49069 Osnabrück, Germany†

E-mail: hjreyher@physik.uni-osnabrueck.de

Received 15 September 2000, in final form 3 November 2000

Abstract. A cubic and an axial Fe^{2+} centre, Fe^{2+}_{Ta} and Fe^{2+}_{Ta}–V_O, are found in reduced Fe-doped $KTaO_3$ crystals in conjunction with their trivalent partners. These four defects are characterized by optically detected magnetic resonance (ODMR) via the magnetic circular dichroism (MCD) of the absorption. The g-values are determined by and interpreted using crystal-field terms. For all centres, the optical absorption bands are identified by the tagged-MCD method. The main MCD bands of the divalent ions are attributed to the well known $^5T_2 \rightarrow {}^5E$ crystal-field transition in the 10 000 cm^{-1} region. Bands at higher energies are interpreted as intervalence transfer transitions to conduction band-like states.

1. Introduction

It is known that defect centres play a decisive role in determining the properties of crystalline materials in general and, in particular, the optics of photorefractive oxides [1]. A good example for the latter is the famous Fe^{2+}/Fe^{3+} recharging process in $LiNbO_3$, possibly the best understood basic mechanism in photorefractive materials [2]. Since iron is frequently observed as an impurity in many oxides, and since Fe^{2+} is well known to exhibit broad absorption in the visible, this ion is often held to be responsible for unintentional coloration of otherwise colourless crystals. Therefore, it seems to be important to collect as much information as possible on Fe^{2+} in oxide hosts, especially if these species and their optical bands can be identified unambiguously, as is the case here for the model substance $KTaO_3$.

In addition, interest arises from the continuing discussion on iron centres in $KTaO_3$. In fact, rarely have so many different Fe-related defect centres been identified in a single host crystal. The literature reports on cubic Fe^{3+}_{Ta} and Fe^{3+}_{K} [3, 4], axial Fe^{3+}_{Ta}–V_O, Fe^{3+}_{K}–O_I [5, 6] and the same species in the charge state 4+ [7, 8], and an Fe^{3+} centre showing orthorhombic symmetry [9, 10]. Also, axial iron with spin $S = \frac{3}{2}$, Fe^{+} and/or Fe^{5+}, is observed [7, 10]. It seems therefore valuable to extend this list by adding the Fe^{2+} centres described below and to characterize the optical bands of the trivalent partner centres as well. The explicit identification of optical bands of Fe^{3+} centres in materials of relatively low band gap, such as $KTaO_3$, is also important, since the indistinct yet often observed increasing absorption near the band edge is attributed to these species without further evidence.

In early EPR work, appreciable attention has been paid to the peculiar properties of Fe^{2+} in an octahedral field [11]. As this kind of defect is detected only in a few cases, it is worth

† Fax: +49-541-9692670.

0953-8984/00/5010599+12$30.00

discussing the g-value of Fe^{2+}_{Ta} in $KTaO_3$ in comparison. Also, the paramagnetic properties of Fe^{2+}_{Ta}–V_O in $KTaO_3$ are quite interesting, as we can show that in this case the tetragonal orbital doublet ^5E is the ground state. This differs from the case for other hosts, e.g., the related crystal $SrTiO_3$ [12] or $LiNbO_3$ [13], where the orbital singlet $^5B_2$ is the lowest.

2. Experimental procedure

The potassium tantalate crystals were grown at the Crystal Growth Laboratory of Dr Hesse at the Physics Department in Osnabrück using the 'top-seeded solution growth' technique. Samples from five different boules were investigated, with iron content between 2500 and 20 000 ppm in the melt. The crystals were brown or greyish in colour and showed almost unstructured absorption in the visible and near-infrared spectral region. As a rule, several iron centres are simultaneously present, depending on the redox treatments and/or illumination by UV light at low temperatures. Table 1 displays information on the treatment of those crystals in which the Fe^{2+} centres under discussion were seen. After UV exposure, an O^- centre was generally observed in addition [30].

Table 1. Treatment parameters for those $KTaO_3$:Fe crystals in which the Fe^{2+} centres were observed. ◇: centre observed after UV illumination at 4 K.

Crystal, [Fe] in the melt	Treatment	Centres observed
R17, 5000 ppm	H_2, 19 h, 800 °C	Cubic Fe^{3+}_{Ta}, Fe^{2+}_{Ta}; axial Fe^{3+}–V_O, Fe^{3+}–O_I, Fe^{2+}–V_O
R129, 2500 ppm	H_2O, 8 h, 900 °C	Axial Fe^{3+}–V_O, Fe^{3+}–O_I, Fe^{2+}–V_O
R126, 2500 ppm	H_2O, 8 h, 900 °C	Axial Fe^{3+}–V_O, Fe^{3+}–O_I◇, Fe^{2+}–V_O◇

In conjunction with table 1, it is interesting to note that oxidization and reduction treatments of $KTaO_3$ are rather subtle processes and very sensitive to the specific treatment conditions. Also, the crystals grow individually and virtually identical specimens exhibit different Fe-centre scenarios, even if chemically treated together. This has been observed in quite a number of cases [14]. It is therefore not surprising that we found, e.g., cubic Fe^{3+}_{Ta} only in one crystal reduced in a hydrogen atmosphere, whereas in earlier work [15] this centre was created easily by reduction in H_2O vapour. Similarly, cubic Fe^{3+}_K [3] was never observed in our experiments (including conventional EPR ones). This great defect diversity is common to many related oxides [1] and constitutes a severe problem for application-oriented work.

The MCD and the ODMR measurements as well as the observations of photochromism were performed with a standard set-up as described, e.g., in reference [16]. Three different detectors were used for the MCD probe light: a red-sensitive photomultiplier, a silicon diode, and a cooled germanium diode. Having sufficiently overlapping sensitivity regions, these detectors allow one to cover the spectral region displayed in the figures below. Illumination of the sample in the cryostat for recharging was performed mainly using a xenon arc lamp with a broad-band UV filter (Schott UG11). All recharging experiments were performed at low temperature ($T < 4.2$ K) and the species generated were metastable at this T. Microwave radiation at 35 and 70 GHz used to induce the magnetic resonance transitions was applied to the sample by a WR28 waveguide. This radiation can be switched on and off to measure the tagged-MCD spectra [16]. By this technique, the spectral dependence of the *change* of the MCD caused by EPR transitions (i.e., the ODMR signal) is recorded. A tagged-MCD spectrum therefore reflects the MCD bands of the specific centre at resonance. The sign of the tagged-MCD bands is the same as that of the corresponding MCD bands, which, in turn, is checked by a circular analyser of known sense.

3. Results and discussion

3.1. Cubic Fe_{Ta} centres

As already mentioned, astonishingly only in one reduced specimen (table 1) were cubic Fe_{Ta} centres observed by means of ODMR (figure 1). Only the 3+ centre is also detected by means of conventional EPR. The latter centre is easily identified by its characteristic fine-structure pattern, and good agreement with the known [3] EPR parameters was found by analysing the angular dependence of the ODMR signals.

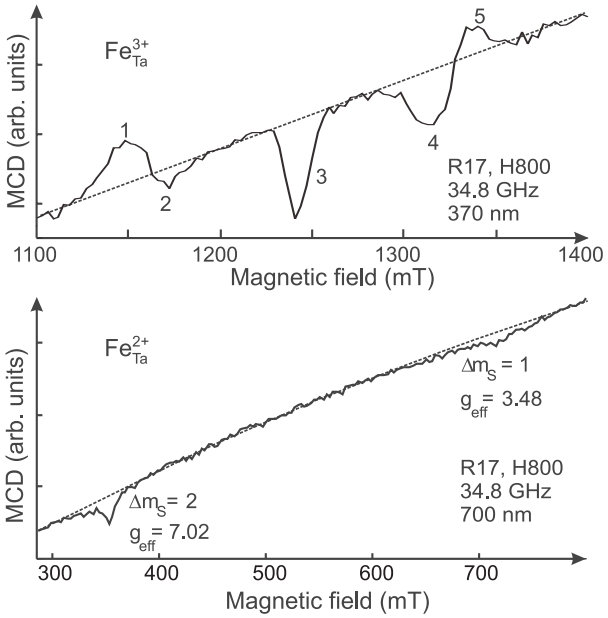

Figure 1. ODMR spectra of cubic Fe^{3+}_{Ta} and Fe^{2+}_{Ta} in $KTaO_3$. In both cases the MCD without microwaves is sketched as a guide to the eye. The different signs of the two lines of the classical Fe^{3+} fine structure can be understood by considering MCD selection rules and the irreducible representations of the Zeeman sublevels [14]. For Fe^{2+} the forbidden $\Delta m_s = 2$ resonance is also shown. The strength of this line is due to poor microwave polarization in our set-up using no cavity. For the same reason, $\Delta m_s = 2, 3, 4, 5$ transitions could be observed for Fe^{3+}_{Ta}.

The cubic centre Fe^{2+}_{Ta} is identified by a number of indications, to be discussed in the following. First, we observe an isotropic resonance and a characteristic g-value of approximately 3.5. This value is predicted by crystal-field theory [11] for a d^6 ion if the octahedral environment is preserved against a Jahn–Teller distortion through spin–orbit coupling and if the factor k of orbital reduction due to covalency is set equal to 1. The only slight deviation, $\delta g_{\mathrm{exp}} = 3.5 - g_{\mathrm{exp}} = 0.02(2)$, is interesting if compared to that for the extensively discussed case of Fe^{2+} in MgO. There, $\delta g = 0.07$ is found, leading to the estimate $k \approx 0.8$ [11]. In our case, however, δg_{exp} can be explained with $k \approx 1$. The correction δg arises from a spin–orbit admixture of the excited $^5\mathrm{E}$ with the $^5\mathrm{T}_2$ ground state:

$$\delta g = -\frac{18}{5}\frac{\lambda}{10Dq}k^2$$

(see reference [11], neglecting possible anisotropy of λ and k). With $10Dq \approx 12\,000\ \mathrm{cm}^{-1}$ for the energy distance $\varepsilon(^5\mathrm{E}) - \varepsilon(^5\mathrm{T}_2)$ from our optical data (see below) and the free-ion

value $\lambda \approx -100\,\mathrm{cm}^{-1}$, we find $\delta g = 0.03$, which agrees with δg_{exp} within experimental error. The finding $k \approx 1$ for $KTaO_3$ is surprising, as this host is reputed to be a strongly covalent substance [17].

The attribution of the resonances in the lower part of figure 1 to Fe^{2+}_{Ta} is further supported by the characteristic optical bands of the MCD when tagged to these two ODMR lines (see below), and also by the observation of the typical forbidden transitions at half the field of the allowed resonance [11]. As usual, a random distribution of small axial strain fields may be invoked to account for the very large width of the $\Delta m_S = 1$ transition and the much smaller $\Delta m_S = 2$ resonance. Finally, as another indication, we remark that under UV illumination the intensity of the ODMR signals from Fe^{2+}_{Ta} increased while that of the signals from Fe^{3+}_{Ta} decreased simultaneously. This recharging could be partly reversed by illuminating the crystal at 700 nm. When recharging Fe^{3+}_{Ta} to Fe^{2+}_{Ta}, holes trapped at any defects of unknown nature must be generated. The 700 nm radiation may free these trapped holes and thus allow recombination with Fe^{2+}_{Ta}, or Fe^{2+}_{Ta} may be photoionized with subsequent photoelectron–hole recombination. The latter process implies that conduction band-like states are energetically close to the Fe^{2+}_{Ta} crystal-field state excited at 700 nm (see below). Some evidence that this is so may be deduced from the MCD spectrum of Fe^{2+}_{Ta}, which we shall present and discuss now.

Figure 2 shows the tagged-MCD spectra of both cubic iron centres. The values on the ordinate correspond to the height of the ODMR signal of the relevant ion. As both species were simultaneously present in our crystal R17, the spectra demonstrate the selectivity of the tagged-MCD method for isolated, uncoupled centres.

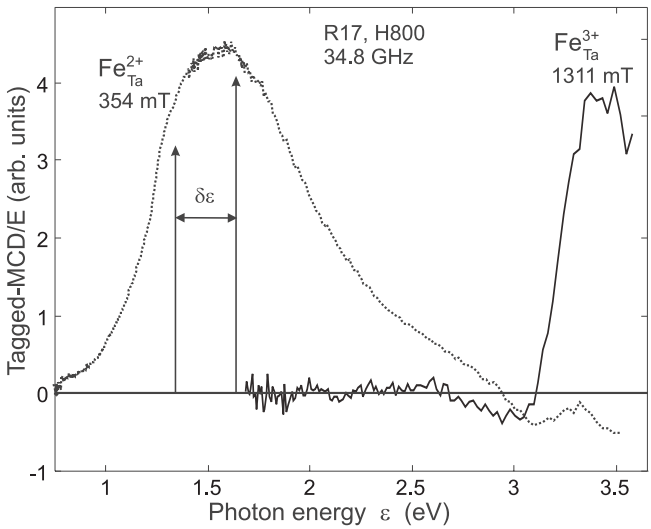

Figure 2. Tagged-MCD spectra of cubic Fe^{3+}_{Ta} and Fe^{2+}_{Ta} in $KTaO_3$. The resonance fields used are indicated. The spectral intensity has been divided by the photon energy to reveal the true band shapes [18]. In the case of Fe^{2+}_{Ta}, the spectral range had to be extended into the NIR. Three types of detector were used, whose sensitivity ranges overlap in the region around 1.6 eV. The weak negative band of Fe^{3+}_{Ta} at 3.1 eV has been verified by recording ODMR spectra there. Note that the height of a tagged-MCD band depends on the specific conditions for ODMR of the centre at resonance. Hence, for the two centres concerned, arbitrary and individual scales are used.

The tagged MCD of Fe^{3+}_{Ta} shows a strong band beyond 3.4 eV and a weak negative one, most probably centred around 3.2 eV and extending down to the yellow spectral region. It is difficult to assign band maxima here, because the extrema of the measured spectrum result from

a superposition of positive and negative MCD bands (the 'pseudo-A' bands of reference [19]). This situation is typical for the MCD of broad-band systems, like that of d ions in oxides. The maxima of the corresponding absorption bands can only be estimated if most of the spectral range covered can be investigated. Here, for Fe^{3+}_{Ta}, the possibility cannot be excluded that further bands exist beyond our detection limit (≈3.5 eV given by strongly increasing absorption) and that the maximum of the Fe^{3+}_{Ta} absorption in $KTaO_3$ is at similar energies to those found for other oxides, e.g., 4.35 eV for MgO [20] and 4.8 eV for Al_2O_3 [21]. These Fe^{3+} bands are assigned to a ligand-to-metal charge-transfer transition. It is difficult to develop a reliable model to predict the MCD of such a transition and we therefore cannot comment further on the MCD spectra of Fe^{3+}_{Ta}.

The main bands of the tagged MCD of Fe^{2+}_{Ta} peaking around 1.5 eV are easily attributed to the well known $T_2 \rightarrow E$ crystal-field (CF) transition of this ion in octahedral coordination. Two subbands can be identified with peaks, as indicated by arrows in figure 2. The mean position at 12 100 cm^{-1} = 1.5 eV and the splitting $\delta\varepsilon \approx 2400$ cm^{-1} = 0.3 eV both fit well into the data set from the classical work on absorption of Fe^{2+} in various hosts by Jones [22]. The asymmetry of the whole structure may also be seen in the absorption spectrum of Fe^{2+} in $KMgF_3$ shown by Jones or that of MgO:Fe^{2+} [23]. This feature has been treated theoretically by Slonczewski [24]. The double-peak structure seen for the systems just mentioned is absent for $KTaO_3$, presumably because the width of the two components is larger, as one may estimate from the total width of the band.

In contrast to the situation concerning Fe^{3+}_{Ta} discussed before, the absorption and the MCD spectra for the $T_2 \rightarrow E$ CF transition are assumed to have the same shape. In other words, we expect both of the MCD subbands resulting from the strong Jahn–Teller coupling in the excited E state to have the same sign and, moreover, the same ratio of intensities as the bands observed in absorption. This postulate is supported by an experimental finding and by theoretical arguments. We start with the latter. From theoretical work (e.g., [26]) we know that the band shape is determined by overlap integrals of the vibrational parts of the ground-state wave function and the wave functions which belong to the upper and the lower sheet of the 'Mexican hat', which constitute the energy surfaces of the excited vibronic E states. The electronic part of the wave function is the same for both sheets when one averages over all positions in the (Q_2, Q_3)-space spanned by the normal coordinates of the E mode. Therefore, the averaged MCD-relevant electronic matrix elements (electric or magnetic dipole operators; see reference [23]) must be the same for transitions to both sheets of the Mexican hat. Although the cited work [26] refers to cubic sites (without dynamic symmetry lowering), the arguments given are valid for the trigonal group C_{3v} as well, as one may verify by inspecting a point group table. It is therefore justified to cite experimental results on Al_2O_3:Ti as further supporting evidence. Ti–sapphire for laser applications is one of the purest systems available and the bands corresponding to the $T_2 \rightarrow E$ CF transition of Ti^{3+} can be measured with negligible background absorption [25]. We can therefore compare absorption and MCD bands easily in this case. Figure 3 depicts the MCD and Ti^{3+}-tagged MCD for a doubly doped crystal, Al_2O_3:Ti:Fe.

This figure, which in addition demonstrates the selectivity of the tagged-MCD method, proves the equality of MCD and absorption bands [25] for the Jahn–Teller-split $T_2 \rightarrow E$ transitions. Comparing the position, width and relative height of the MCD bands with absorption data from the literature [25], we find excellent agreement.

In figure 2 small negative MCD bands are present in the spectrum of $KTaO_3$:Fe^{2+}_{Ta} beyond 3 eV and there may also be a weak additional positive band at ≈2.7 eV overlapping the wing of the $T_2 \rightarrow E$ band. Similar additional bands are not seen in the tagged-MCD spectrum of Al_2O_3:Ti^{3+} where the crystal-field band is isolated. We attribute these extra MCD bands to

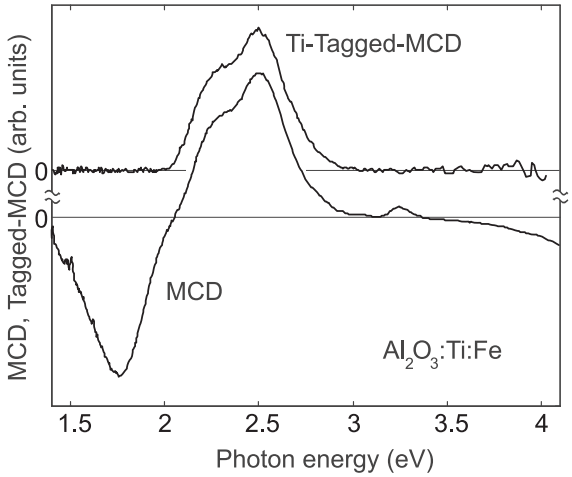

Figure 3. MCD and Ti^{3+}-tagged-MCD spectra of an Al_2O_3 crystal containing titanium and iron. The tagged MCD shows exactly the same band properties of the $T_2 \rightarrow E$ transitions of Ti^{3+} as were found by simple absorption spectroscopy for pure Ti–sapphire laser crystals. The filter effect of the tagging method is clearly visible.

intervalence transfer transitions, i.e., to transitions to states with conduction band character (Ta-like). This is plausible since the band gap of $KTaO_3$ is much narrower than that of Al_2O_3 and considerable absorption was observed above 3.5 eV for all of our samples. The proximity of conduction band-like excited states to the excited crystal-field E state also allows an easy explanation of our observation that Fe^{2+}_{Ta} can be recharged to the 3+ state by 700 nm light (1.77 eV), as mentioned above. Energetically adjacent conduction band-like states are a prerequisite for channels of relaxation from the localized E state to extended states allowing carrier transport. Photoionization of Fe^{2+}_{Ta} may occur in this way by excitation within a crystal-field band. The intervalence transfer transitions are much stronger for the axial counterpart of Fe^{2+}_{Ta}, which we will discuss now.

3.2. Axial Fe_{Ta}–V_O centres

The existence of an axial (tetragonal) centre, Fe^{3+}_{Ta}–V_O, in $KTaO_3$ and its distinction from Fe^{3+}_{K}–O_I were established by EPR work in combination with redox treatments [6]. The centres have different effective g-values $g^{\rm eff}_{\perp}$ for the magnetic field $\vec{B}$ oriented perpendicular to the centre axis. One finds at 35 GHz $g^{\rm eff}_{\perp} = 6$ and $g^{\rm eff}_{\perp} = 5.8$ for Fe^{3+}_{K}–O_I and Fe^{3+}_{Ta}–V_O, respectively. In conjunction (see table 1) with the signal for Fe^{3+}_{Ta}–V_O identified in this way, a new ODMR signal appears for reduced samples. We shall attribute this signal to Fe^{2+}_{Ta}–V_O. This species is, to our knowledge, not described in the literature and is identified by several observations.

First, the associated ODMR signal can be increased by UV illumination at the expense of the signal from Fe^{3+}_{Ta}–V_O. This is similar to the cubic case discussed above. Partial recharging from the divalent to the trivalent state by 700 nm light is observed here as well. Second, the angular dependence, displayed in figure 4, indicates an axial ($S = 2$) ion. At the low temperatures used, only one ODMR transition for each magnetically inequivalent centre can be detected. In order to distinguish the centre under discussion from the other known

($S = 2$) centre (Fe^{4+}_{ax})† in $KTaO_3$, the angular dependence was fitted taking the same spin Hamiltonian [11] as was used for Fe^{4+}_{ax}:

$$\mathcal{H} = g\beta\vec{B}\cdot\vec{S} + D\left(S_z^2 - \frac{1}{3}S(S+1)\right) + \frac{a}{120}(O_4^0 + 5O_4^4). \tag{1}$$

In equation (1) the operators $O_4^{0,4}$ are polynomials of spin components [11]. An excellent fit (figure 4) is obtained with the parameters $g = 2.313$ (isotropic), $D \geqslant 15\,\mathrm{cm}^{-1}$ (axial CF), and $a \leqslant 0.0024\,\mathrm{cm}^{-1}$ (cubic CF). The local z-axes of the centres are along $\langle 100\rangle$. Only limits can be given for D and a, but the essential point is that the g-value deduced is quite different from $g \approx 2$, found for Fe^{4+}_{ax}. This clearly distinguishes Fe^{2+}_{Ta}–V_O from Fe^{4+}_{ax} in $KTaO_3$. The above parameters are equivalent to an effective g-value $g_\parallel^{\mathrm{eff}} = 9.33$ for $S^{\mathrm{eff}} = 1/2$ (at 35 GHz) in contrast to $g_\parallel^{\mathrm{eff}} \approx 8$ for Fe^{4+}_{ax}.

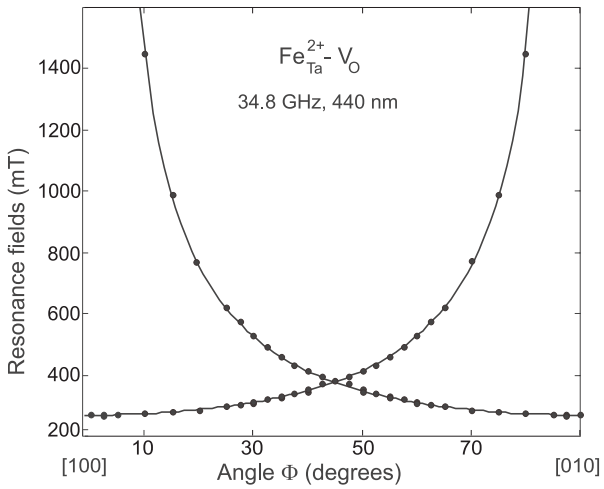

Figure 4. The angular dependence of the ODMR signals from Fe^{2+}_{Ta}–V_O for a rotation of the magnetic field B in a (100) plane. Dots represent the experimental points; the straight lines are obtained from a fit using equation (1)

The next indication for the presence of Fe^{2+}_{Ta}–V_O consists in the fact that it is possible to find a straightforward interpretation of $g_\parallel^{\mathrm{eff}} = 9.33$ which is in accordance with the optical properties of the centre (see below). The values $g_\parallel^{\mathrm{eff}} = 9.33$ and $g_\perp^{\mathrm{eff}} \approx 0$ are unusual for d ions [11] in general. For the similar centre in $SrTiO_3$, $g_\parallel^{\mathrm{eff}} \approx 8$ and $g_\perp^{\mathrm{eff}} \approx 0.66$ (at 9.3 GHz) have been found (data from figure 3 of reference [12]).

Assuming the centre Fe^{2+}_{Ta}–V_O, we have to consider an octahedrally coordinated d^6 ion with a ground state of cubic $^5T_2$ symmetry. This state splits in a tetragonal CF, which comes into existence through the oxygen vacancy, into an orbital singlet $^5B_2$ and an orbital doublet $^5E_2$, where the latter symbols indicate representations of the tetragonal group C_{4v} [27]. According to the following, $^5E_2$ is the ground state for Fe^{2+}_{Ta}–V_O. For an interpretation of g^{eff} we need to calculate the Zeeman splitting of the lowest spin–orbital states. In the usual parametrized approach, the full ^5D manifold may be described by a Hamiltonian $\mathcal{H}$ based on equivalent orbital momentum operators O_k^q accounting for the CF, the spin–orbit interaction, and the

† By means of ODMR, we found an $S = 2$ centre which we termed Fe^{4+}_{K}–O_I [8]. Later, a group from St Petersburg presented arguments indicating that the nature of this centre is that of Fe^{4+}_{Ta}–V_O [7].

Zeeman operator [11]:

$$\mathcal{H} = B_4(O_4^0 + 5O_4^4) + B_2^0 O_2^0 + B_4^0 O_4^0 + \lambda \vec{L} \cdot \vec{S} + \mu_B \vec{B} \cdot (2\vec{S} + \vec{L}). \quad (2)$$

Here, $B_4 = 10Dq/120$ stands for the cubic CF parameter, B_2^0 and B_4^0 for the tetragonal part, λ for the spin–orbit coupling constant (negative for a d^6 state), and $\vec{B}$ is the magnetic field. We numerically diagonalized the matrix of $\mathcal{H}$ from equation (2) within the ^{5}D states†. We find, for a wide range of parameters, $g_\parallel^{\text{eff}} = 9$–$10$ and $g_\perp^{\text{eff}} = 0$. For $10Dq$ we used 13 000 cm^{-1} derived from the MCD bands of the CF transitions (see below) and λ was set to -100 cm^{-1}. From reference [11], we find for the tetragonal splitting Δ_{T_2} of the cubic T_2 ground state $\Delta_{T_2} = 9B_2^0 + 60B_4^0$. One obtains the observed $g_\parallel^{\text{eff}} = 9.3$ for any combination of B_2^0 and B_4^0 which yields $\Delta_{T_2} \approx 470$ cm^{-1}. From the interpretation of the MCD spectra given below, we find explicitly $B_2^0 = -48$ cm^{-1} and $B_4^0 = +15$ cm^{-1}. Irrespective of the parameter set chosen, the calculation proves quite generally the compatibility of the model for Fe_{Ta}^{2+}–V_O with the observed effective g-values. The experimental finding $g_\perp^{\text{eff}} = 0$ and $g_\parallel^{\text{eff}} = 9.3$ *cannot* be explained by a CF approach for any other splitting sequence of a ^{5}D system, be it d^4 or d^6.

The tagged-MCD spectrum of the Fe_{Ta}^{2+}–V_O centre is shown in figure 5, again together with its trivalent counterpart which will be briefly discussed first.

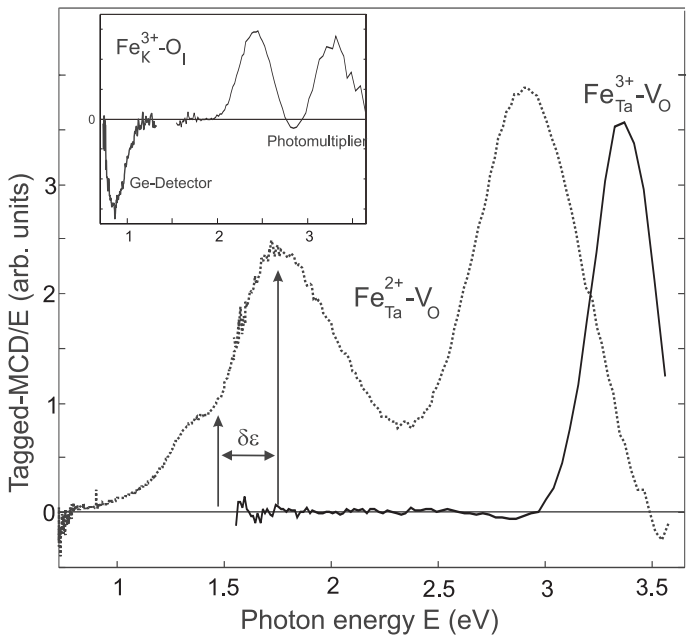

Figure 5. Tagged-MCD spectra of axial Fe_{Ta}^{3+}–V_O and Fe_{Ta}^{2+}–V_O. The additional remarks from the caption of figure 2 apply similarly. Tagged-MCD spectra of Fe_K^{3+}–O_I are shown in the inset for comparison (see the text).

It is interesting to note that the MCD of Fe_{Ta}^{3+}–V_O has a structure which is practically identical to that of its cubic trivalent partner. Also the weak negative band extending down to 2.7 eV is present. The whole feature is merely shifted by ≈0.1 eV to the red. This similarity

† Omitting the tetragonal B_4^0-term and restricting $\vec{B}$ to being parallel to the fourfold centre axis, Low and Weger [28] have calculated the energy levels of the system analytically using perturbation theory. To avoid the limitations of this approach, we made a numerical calculation.

indicates that the states involved in the charge-transfer transition of Fe^{3+} are only weakly affected by the oxygen vacancy. This is plausible for the Fe-like final state, but somewhat surprising for the oxygen-like initial state. If the initial state is modelled as, e.g., a molecular orbital, it should be altered substantially when the ligand coordination is changed. As an example of a modification of the optical properties of Fe^{3+} caused by modifying the oxygen environment, we may cite the tagged MCD of Fe^{3+}_{K}–O_I [29]. Here, intense bands in the red and near-IR region can be seen in addition to the typical Fe^{3+} structure discussed before. The latter bands are still further red-shifted for this centre (see the inset of figure 5). It seems challenging to investigate these findings by means of suitable quantum-chemical calculations.

Figure 5 depicts the tagged-MCD spectrum of Fe^{2+}_{Ta}–V_O. The bands between 1 and 2.5 eV are similar to those of cubic Fe^{2+}_{Ta} and are again attributed to the $^5T_2 \rightarrow {}^5E$ CF transition. We shall discuss these MCD bands in the next paragraph. At 2.9 eV a relatively strong positive band shows up which is absent in the case of cubic Fe^{2+}. We interpret this band as arising from an Fe–Ta intervalence transfer (IT) transition—that is, in the same way as the weak negative band at 3.1 eV of cubic Fe^{2+} (see the end of the last section)†. Obviously, the presence of the symmetry-lowering oxygen vacancy induces an additional IT transition with an associated strong positive MCD band which superposes on the possibly still present IT bands observed in the cubic case (at 2.7 and above 3 eV). In other words, localized tantalum-like or conduction band-like states which are absent for the isoelectronic cubic centre come into existence through the perturbation caused by V_O. In an alternative interpretation, the MCD band of Fe^{2+}_{Ta}–V_O might be attributed to an iron internal transition to a 4p-like state. However, in view of the high energy of 4p states of the free iron ion [31], the explanation mentioned before should be preferred.

In the following, the MCD structure of the region dominated by CF transitions (1–2.3 eV) is analysed using group theory. If we confine the discussion to the case where $\vec{B}$ is parallel to the fourfold axis of Fe^{2+}_{Ta}–V_O, we have to consider the point group C_4 (C_{4v} without $\vec{B}$). In this group it is particularly simple to predict MCD bands since all irreducible representations (irreps) may be considered as one-dimensional ones and the coupling coefficients reduce to one [27]. From the g-value analysis above, we have sufficient information on the lowest Zeeman level of the ground-state Kramers doublet, i.e., we know its spin–orbit composition. As this level, transforming as ^1E, is mainly occupied at the low temperatures used in the experiment, it is sufficient to analyse the selection rules for left- and right-circular-polarized electric dipole transitions starting from ^1E to the excited orbitals transforming as A(E) and B(E) (figure 6(a)). We label the irreps according to reference [27] with the cubic parent irreps in brackets. Some details are given in the appendix. The result is that the MCD for $^1E \rightarrow A$ is positive while that for the transition $^1E \rightarrow B$ is negative (figure 6). This result does not depend on the (unknown) reduced matrix elements which are independent of each other for each transition and which determine the strength of the corresponding MCD band. As a consequence, a derivative-like structure should appear if the two bands have similar widths and intensities. The situation is illustrated by figure 6(b) for the case of B(E) lying above A(E).

This is clearly not observed. However, in the odd crystal field from the V_O perturbation, one may, as usual, assume that the d–d transitions become electric dipole allowed by 4p admixture with the excited state. Since the presumably lowest $4p_z$ orbital transforms according to A, 4p admixture occurs mainly for the excited A state and leads to a larger MCD for $^1E \rightarrow A$ compared to $^1E \rightarrow B$. This may lead to a fully positive CF band of Fe^{2+}_{Ta}–V_O. In this interpretation, the bump at 1.5 eV (figure 5) comes from a small negative band associated

† The intensities of tagged-MCD spectra for different centres cannot be compared in a straightforward manner, since they depend on the particular strength of the ODMR line which is used for the tagging. Therefore arbitrary units are used and only the relative intensity of CF and IT bands for each centre is meaningful.

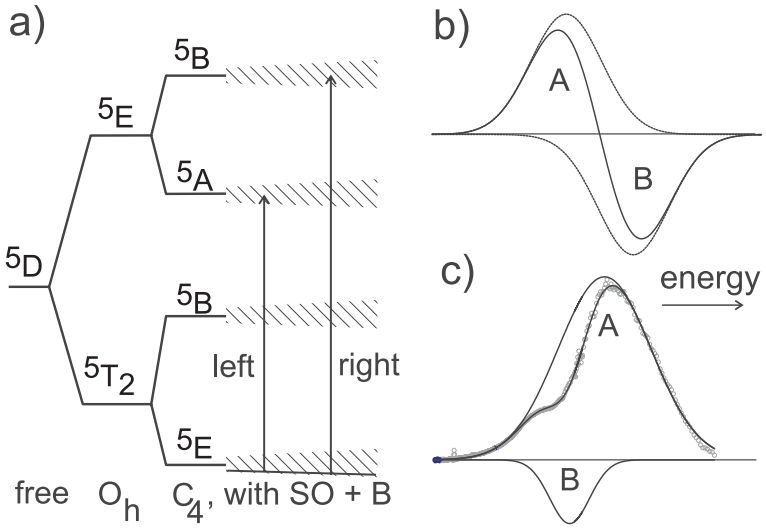

Figure 6. The interpretation of the MCD of the crystal-field transitions of Fe^{2+}_{Ta}–V_O. (a) The splitting diagram. In the region with spin–orbit (SO) coupling and the magnetic field B, the level manifolds are represented by hatched regions. (b) The MCD structure expected for equal strength of left- and right-polarized transitions and level B above A. (c) The fit to the tagged-MCD data with the proposed MCD structure (see the text).

with the transition $^1E \rightarrow B$ (see figure 6(c)). To fit the observed structure in this way we also require that the axial field inverts the sequence of B(E) and A(E). This can be realized for the parameter set $B^0_2 = -48\,cm^{-1}$ and $B^0_4 = +15\,cm^{-1}$ which simultaneously yields the observed effective g-values, as mentioned above.

The postulated MCD structure raises some open questions. First it requires for the widths W of the subbands $W(B) \ll W(A)$. No argument supporting this can be given at present. Second, if one inverts the negative MCD band to obtain an estimate for the associated absorption band, one finds that the characteristic double structure known to occur for other hosts [22] will not be well resolved. This is mainly due to the large width of the subband A and contradicts naive expectation. From the substantial axial perturbation of the oxygen vacancy, one anticipates a much larger splitting than that resulting from the dynamic interaction in the case of the cubic centre Fe^{2+}_{Ta}. Explaining these details represents a hard test for advanced theoretical descriptions. An experimental verification of the absorption structure predicted by the MCD interpretation was not possible, unfortunately. Numerous bands were present for our crystals and only nearly unstructured absorption was observed.

4. Conclusions

Iron-ion impurities form an important class of defect centres in oxides. The combination of magnetic resonance with optical spectroscopy allows the submicroscopic characterization of divalent and trivalent iron defects in $KTaO_3$ as well as the attribution of optical bands to the corresponding species. The very detailed information on the magnetic and optical properties for the set $Fe^{2+/3+}_{Ta}$ and $Fe^{2+/3+}_{Ta}$–V_O facilitates a systematic study of the influence of the axial perturbation on the optical bands. The MCD bands show partially a very similar character for the cubic and the axial ion, whereas the magnetic ground-state properties of the same species

are very different. This is simply a consequence of the fact that unlike quantities are measured by optical and magnetic resonance methods. Only by means of combined spectroscopies, like in the MCD–ODMR method, can a consistent picture of the defect scenario can be obtained.

Appendix

To consider the MCD using group theory we start with the ground state. We know from its magnetic resonance that it must be a Kramers doublet. In C_4 this means that its Zeeman components transform as ^{1}E and ^{2}E. The multiplication table gives for the lowest ^{1}E spin orbital

$$|^1\mathrm{E}\rangle = i_1|1\rangle|0\rangle + i_2|-1\rangle|2\rangle + i_3|-1\rangle|-2\rangle = i_1|^1\mathrm{E}\rangle|\mathrm{A}\rangle + i_2|^2\mathrm{E}\rangle|\mathrm{B}\rangle + i_3|^2\mathrm{E}\rangle|\tilde{\mathrm{B}}\rangle.$$

The transformation properties [27] of the spin and orbital components $M_S = 2, \ldots, -2$ and $M_L = \pm 1$ can be read from this equation. The large magnetic moment of the corresponding state ($g_{\mathrm{eff}} = 9.3$!) stems from the component with the coefficient i_3, which is highly dominant as found in our numerical calculations. Admixtures of excited orbitals are very small and may be neglected. The operators of electric dipolar MCD, $x \pm \mathrm{i}y$, transform as ^{1}E and ^{2}E. The wave functions of the excited states A(E) and B(E) are suitable combinations of orbitals $|\mathrm{A}\rangle = |0\rangle$ and $|\mathrm{B}\rangle = (1/\sqrt{2})(|2\rangle + |-2\rangle)$ with the spin functions $M_S = 2, \ldots, -2$. In calculating the MCD one sums over all exited states [19]. As the operators do not act on the spin and as i_3 is dominant, only the spin components $M_S = -2$ of the excited states are relevant. The multiplication table of C_4 then yields

$$\mathrm{MCD}(^1\mathrm{E} \to \mathrm{A}) \propto |\langle \mathrm{A}\|^1\mathrm{E}\|^2\mathrm{E}\rangle|^2 \qquad \mathrm{MCD}(^1\mathrm{E} \to \mathrm{B}) \propto -|\langle \mathrm{B}\|^2\mathrm{E}\|^2\mathrm{E}\rangle|^2.$$

These two reduced matrix elements are independent of each other.

Acknowledgments

We thank Professor O F Schirmer for active help and fruitful discussions. The supply of samples by Dr H Hesse and his group is greatly appreciated. This work was supported by the Deutsche Forschungsgemeinschaft, SFB 225/C4/C2.

References

[1] Schirmer O F, Reyher H-J and Wöhlecke M 1995 *Insulating Materials for Optoelectronics* ed F Agulló-López (Singapore: World Scientific) ch 4
[2] Kurz H, Krätzig E, Keune W, Engelmann H, Gonser U, Dischler B and Räuber A 1977 *Appl. Phys.* **12** 355
[3] Hannon D M 1967 *Phys. Rev.* **164** 366
[4] Rytz D, Höchli U T, Müller K A, Berlinger W and Boatner L A 1982 *J. Phys. C: Solid State Phys.* **15** 3371
[5] Bykov I P, Glinchuk M D, Karmazin A A and Laguta V V 1983 *Sov. Phys.–Solid State* **25** 2063
[6] Laguta V V, Glinchuk M D, Karmazin A A, Bykov I P and Syrnikov P P 1985 *Sov. Phys.–Solid State* **27** 1328
[7] Azamat D V, Basun S A, Bursian V E, Razdobarin A G, Sochava L S, Hesse H and Kapphan S 1999 *Phys. Solid State* **41** 1303
[8] Faust B, Reyher H-J and Schirmer O F 1996 *Solid State Commun.* **98** 445
[9] Pechenyi A P, Glinchuk M D, Antimirova T and Kleemann W 1992 *Phys. Status Solidi* b **174** 325
[10] Reyher H-J, Faust B, Maiwald M and Hesse H 1996 *Appl. Phys.* B **64** 331
[11] Abragam A and Bleaney B 1970 *Electron Paramagnetic Resonance of Transition Ions* (London: Clarendon)
[12] Berney R L and Cowan D L 1981 *Phys. Rev.* B **23** 37
[13] Juppe S and Schirmer O F 1990 *Solid State Commun.* **76** 299
[14] Hausfeld N 1999 *ODMR-Untersuchungen an Kaliumtantalat und Yttrium–Aluminium-Granat* (Aachen: Shaker) Hausfeld N 1999 *Thesis* Universität Osnabrück
[15] Gonzales R, Abraham M M, Boatner L A and Chen Y 1983 *J. Chem. Phys.* **78** 660

[16] Spaeth J-M, Niklas J R and Bartram R H 1992 *Structural Analysis of Point Defects in Solids* (Berlin: Springer) ch 9
[17] Neumann T, Borstel G, Scharfschwerdt C and Neumann M 1992 *Phys. Rev.* B **46** 10 623
[18] Wojtowicz A J, Kazmierczak M, Lempicki A and Bartram R H 1989 *J. Opt. Soc. Am.* B **6** 1106
[19] Stephens P J 1976 *Adv. Chem. Phys.* **35** 197
[20] Modine F A, Sonder E and Weeks R 1977 *J. Appl. Phys.* **48** 3514
[21] Tippins H H 1970 *Phys. Rev.* B **1** 126
[22] Jones G D 1967 *Phys. Rev.* **155** 259
[23] Hjortsberg A, Nygren B, Vallin J and Ham F S 1977 *Phys. Rev. Lett.* **39** 1233
[24] Slonczewski J C 1963 *Phys. Rev.* **131** 1596
[25] Powell R C 1998 *Physics of Solid-State Laser Materials* (Berlin: Springer)
[26] O'Brien M C M 1965 *Proc. Phys. Soc.* **86** 847
[27] Altmann S L and Herzig P 1994 *Point-Group Theory Tables* (Oxford: Clarendon)
[28] Low W and Weger M 1960 *Phys. Rev.* **118** 1119
[29] Reyher H-J, Faust B, Käding M, Hesse H, Ruža E and Wöhlecke M 1995 *Phys. Rev.* B **51** 6707
Reyher H-J, Faust B, Käding M, Hesse H, Ruža E and Wöhlecke M 1996 *Phys. Rev.* B **54** 3662 (erratum)
[30] Reyher H-J *et al* 2000 unpublished
[31] *NIST data* http://physics.nist.gov/PhysRefData/contents.html